

Order parameter fluctuations in natural time and b -value variation before large earthquakes

P. A. Varotsos,^{1,*} N. V. Sarlis,¹ and E. S. Skordas¹

¹*Solid State Section and Solid Earth Physics Institute,
Physics Department, University of Athens,
Panepistimiopolis, Zografos 157 84, Athens, Greece*

Abstract

Self-similarity may stem from two origins: the process' increments infinite variance and/or process' memory. The b -value of the Gutenberg-Richter law comes from the first origin. In the frame of natural time analysis of earthquake data, a fall of the b -value observed before large earthquakes reflects an increase of the order parameter fluctuations upon approaching the critical point (mainshock). The increase of these fluctuations, however, is also influenced from the second origin of self-similarity, i.e., temporal correlations between earthquake magnitudes. This is supported by observations and simulations of an earthquake model.

PACS numbers: 91.30.Dk, 05.40.-a, 64.60.av, 89.75.Da

A large variety of natural systems exhibit irregular and complex behavior which at first look seems to be erratic, but in fact possesses scale-invariant structure, for example see Refs. [1, 2]. A stochastic process $X(t)$ is called self-similar[3] with index $H > 0$ if it has the property

$$X(\lambda t) \stackrel{d}{=} \lambda^H X(t) \quad \forall \lambda > 0. \quad (1)$$

where the equality concerns the finite-dimensional distributions of the process $X(t)$ on the right- and the left-hand side of the equation (*not* the values of the process).

A point of crucial importance in analyzing data from complex systems that exhibit scale-invariant structure, is the following: In several systems this nontrivial structure stems from long-range *temporal* correlations; in other words, the self-similarity originates from the process' memory *only*. This is the case for example of fractional Brownian motion. Alternatively, the self-similarity may solely come from the process' increments *infinite* variance. Such an example is Lévy stable motion (the variance of Lévy stable distributions is infinite since they have heavy tails[4], thus differing greatly from the Gaussian ones). In general, however, the self-similarity may result from both these origins[5], the presence of which can be in principle identified when analyzing the complex time series in terms of the new time domain termed natural time[6].

The evolution of seismicity is a typical example of complex time series. Several traditional studies were focused on the variation of the b -value of the Gutenberg-Richter (G-R) law[7], which states that the (cumulative) number of earthquakes with magnitude greater than (or equal to) M , $N(\geq M)$, occurring in a specified area and time is given by

$$N(\geq M) = 10^{a-bM}, \quad (2)$$

where b is a constant, varying only slightly from region to region and the constant a gives the logarithm of the number of earthquakes with magnitude greater than zero[8]. These studies found that the b -value decreases before a large event, e.g., see Ref.[9] (cases where b -value increases prior to and then decreases sharply before a large event have been also reported[10]). Here, considering that the b -value itself solely focuses on the one origin of self-similarity, and in particular the process' increments infinite variance, we show that, when employing natural time analysis, the b -value decrease before large earthquakes reflects an increase of the fluctuations of the order parameter of seismicity when approaching the critical point (mainshock, see below). The whole precursory variation of the order parameter fluctuations, however, is more complex since it captures *both* origins. Temporal correlations between earthquake magnitudes *also* play an important

role in this precursory variation, thus leading to more spectacular results compared to the ones obtained when restricting ourselves to traditional analysis of b -value alone.

For a time series comprising N events, we define[11] the natural time χ_k for the occurrence of the k -th event (of energy Q_k) by $\chi_k = k/N$. We then study the evolution of the pair (χ_k, Q_k) or (χ_k, p_k) , where $p_k = Q_k / \sum_{n=1}^N Q_n$ is the normalized energy released during the k -th event. The quantity $\Phi(\omega)$ is defined by $\Phi(\omega) = \sum_{k=1}^N p_k \exp(i\omega\chi_k)$, where ω stands for the natural angular frequency, and then evaluate the real function $\Pi(\omega) = |\Phi(\omega)|^2$ in the low frequency limit. By considering the Taylor expansion $\Pi(\omega) = 1 - \kappa_1\omega^2 + \kappa_2\omega^4 + \dots$, we find that the approach of a dynamical system to criticality (see Chapter 8 of Ref.[6]) is identified by means of κ_1 , i.e.,

$$\kappa_1 = \langle \chi^2 \rangle - \langle \chi \rangle^2 = \sum_{k=1}^N p_k \chi_k^2 - \left(\sum_{k=1}^N p_k \chi_k \right)^2, \quad (3)$$

which is the variance[6, 11, 12] of natural time weighted for p_k . When Q_k are independent and identically distributed positive random variables, we obtain the “uniform” (u) distribution of p_k , as it was defined in Ref.[13] (see also p.122 of Ref.[6]). In this case, *all* p_k vary around their mean value $1/N$ (cf. since $\sum_{n=1}^N p_n = 1$) and the quantity κ_1 results[13] in $\kappa_u = 1/12$ for large N .

In general, in a complex time series, in order to identify the two origins of self-similarity by means of natural time analysis, we focus on the expectation value $\mathcal{E}(\kappa_1)$ of the variance κ_1 of natural time when sliding a natural time window of length l through a time series of $Q_k > 0$, $k = 1, 2, \dots, N$.

If self-similarity exclusively results from the process’ memory, the $\mathcal{E}(\kappa_1)$ value should *change* to $\kappa_u = 1/12$ for the (randomly) shuffled data. This is the case of the Seismic Electric Signals (SES) activities[14], which are series of low-frequency (≤ 1 Hz) electric signals detected a few to several weeks (up to five months) before an earthquake when the stress in the focal region reaches a *critical* value (and hence long range correlations develop). For example, the three upper channels in Fig.1(b) show three SES activities that preceded major earthquakes in southern, southwestern and western Greece, respectively, as depicted in the map of Fig.1(a). For the sake of comparison, the lowest channel shows an SES activity recorded in northern Greece (close to Thessaloniki). In all these four cases, the analysis of their original data lead to $\kappa_1 \approx 0.07$ (see also below), which turns to $\kappa_u = 1/12$ upon shuffling the data. On the other hand, if the self-similarity results from process’ increments infinite variance *only*, $\mathcal{E}(\kappa_1)$ should be the same (but differing from κ_u) for the original and the (randomly) shuffled data. Finally, when both origins of self-similarity are present, the relative strength of the contribution of the one origin compared to that of the other can

be quantified on the basis of Eqs.(12) and (13) of Ref. [15] (see also Ref.[6]).

In what remains, we focus on complex time series of seismicity. Earthquakes exhibit scaling relations chief among which is the aforementioned G-R law[7]. For reasons of convenience, we write hereafter G-R law of Eq.(2) into the form $N(\geq M) \propto 10^{-bM}$. Considering that the seismic energy E released during an earthquake is related[16] to the magnitude through $E \propto 10^{cM}$, where c is around 1.5, the latter form turns to the distribution,

$$P(E) \propto E^{-\gamma} \quad (4)$$

where $\gamma = 1 + b/1.5$. Hence, $b \approx 1$ means that the exponent γ is around $\gamma=1.6$ to 1.7 , see Table 2.1 of Ref.[6].

The complex correlations in time, space and magnitude of earthquakes have been extensively studied[17–21]. The observed earthquake scaling laws[22] seem to indicate the existence of phenomena closely associated with the proximity of the system to a *critical* point (e.g., see Ref. [18] and references therein). In the frame of natural time analysis, it has been suggested[12] (see also pp.249-254 of Ref.[6]) that the order parameter of seismicity is the quantity κ_1 . The κ_1 value itself may lead to the determination of the occurrence time of the impending mainshock[6, 11, 15, 23] when SES data are available. In particular, when the κ_1 value resulting from the natural time analysis of the seismicity subsequent to the SES recording becomes approximately equal to 0.070, the mainshock occurs within a time window of the order of one week. This has been empirically observed in several cases[11, 15, 23] (see also Chapter 7 of Ref. [6]) including the three major earthquakes of Fig.1(a) that followed the SES activities depicted in Fig.1(b). An example of the κ_1 dynamics after the recording of the SES activity depicted in the third channel of Fig.1(b) until the occurrence of the magnitude 6.4 mainshock on June 8, 2008 (blue star in Fig.1(a)) is given in Ref.[24]. In the lack of SES data, we have to solely rely on the fluctuations of the order parameter of seismicity. Along these lines, we investigated[25] the period before and after a significant mainshock. Time-series for various lengths of W earthquakes that occurred before or after the mainshock have been studied. The probability distribution function (pdf) $P(\kappa_1)$ versus κ_1 was found to exhibit a bimodal feature when approaching a mainshock. To quantify this feature, we considered the *variability* of κ_1 , which is just the ratio

$$\beta \equiv \sigma(\kappa_1)/\mu(\kappa_1), \quad (5)$$

where $\sigma(\kappa_1)$ and $\mu(\kappa_1)$ stand for the standard deviation and the mean value of κ_1 for sliding window lengths $l=6-40$. The bimodal feature reflects that, upon approaching the mainshock (with

the number W of the earthquakes before mainshock decreasing), the variability of κ_1 should increase. This was subsequently confirmed because before the M9.0 devastating Tohoku earthquake in Japan on March 11, 2011, the variability of κ_1 exhibited[26] a dramatic increase.

In addition, we investigated[27] the order parameter fluctuations, but when considering a natural time window of a fixed-length W sliding through a seismic catalog (cf. in general the results of complexity measures when considering $W = \text{const}$ complement[6] those deduced when taking windows of various lengths W). For earthquakes in California and Greece, we found[27] that when W becomes compatible with the lead time of the SES activities (i.e., of the order of a few months), the fluctuations exhibit a global minimum before the strongest mainshock that occurred during a 25- and 10-year period, respectively.

Let us now study the interrelation between the b -value and the variability of κ_1 . In particular, we investigate the expected value of κ_1 when a natural time window length is sliding through randomly shuffled power law distributed energy bursts that obey Eq.(4). In Fig.2, the pdf $P(\kappa_1)$ versus κ_1 is plotted for several b values, an inspection of which reveals that: For high b -values, e.g., for $b=1.5$ and 1.4 , the $P(\kappa_1)$ versus κ_1 curve is almost unimodal maximizing at a value somewhat larger than 0.070, while for smaller b a second mode emerges close to $\kappa_1 \approx 0$ which reflects that the fluctuations of κ_1 are larger. The computed values of the κ_1 variability as a function of the b value are plotted in the inset of Fig.2(b). The general feature of this curve is more or less similar to that observed for example before Tohoku earthquake[26]; quantitative agreement cannot be demanded, however, because *temporal* correlations between the earthquake magnitudes are also present which influence the observed results. This is corroborated by the following results obtained from the Olami-Feder-Christensen (OFC) earthquake model[28]. We preferred to employ this model here, since it has been studied in detail in hundreds of publications, but we clarify that there exist more recent ones, e.g., see Ref.[29] where the primary role of the fault system geometry is emerged.

The OFC model runs as follows: we assign a continuous random variable $z_{ij} \in (0, 1)$ to each site of a square lattice, which represents the local “energy”. Starting with a random initial configuration taken from a uniform distribution in the segment $(0,1)$, the value z_{ij} of all sites is simultaneously increased at a uniform loading rate until a site ij reaches the threshold value $z_{thres}=1$ (i.e., the loading Δf is such that $(z_{ij})_{max} + \Delta f = 1$). This site then topples which means that z_{ij} is reset to zero and an “energy” αz_{ij} is passed to every nearest neighbor, where the coupling parameter α can take values from zero to 0.25 and is the *only* parameter of the model, apart from the edge length L

of the square lattice. If this causes a neighbor to exceed the threshold, the neighbor topples also, and the avalanche continues until all $z_{kl} < 1$. Then the uniform loading increase resumes. The number of topplings defines the size of an avalanche or “earthquake” and (when it is larger than unity k increases by one) is used as Q_k in natural time analysis. Here, we use the case of free boundary conditions[30] in which α varies locally $\alpha_{ij} = \frac{1}{n_{ij}+K}$, where n_{ij} is the actual number of nearest neighbors of the site ij (for sites in the bulk $n_{ij} = 4$, for sites at the edges $n_{ij} = 3$ and for the four sites at the corners $n_{ij} = 2$) and K denotes[30] the elastic constant of the upper leaf springs measured relatively to that of the other springs between blocks in the Burridge-Knopoff model[31]. The OFC model is obviously non-conservative for $K > 0$ for which $\alpha_{ij} < 0.25$ in the bulk (for more details on the OFC modelling see pp. 349-363 of Ref.[6] and references therein).

We first study the predictability of the OFC model on the basis of the κ_1 variability. We consider the variability β_k which is a function of the natural time index k , $k = 1, 2, \dots, N = 2 \times 10^6$ estimated by analyzing in natural time for each k the preceding $W = 100$ avalanches. The time increased probability (TIP)[32] (i.e., the time during which there exists a high probability for the occurrence of a large avalanche exceeding a given threshold) is turned on when $\beta_k > \beta_c$, where β_c is a given threshold in the prediction. If the size Q_k is greater than a target avalanche size threshold Q_c , we have a successful prediction. For binary predictions, the prediction of events becomes a classification task with two types of errors: missing an event and giving a false alarm. We therefore choose[33] the receiver operating characteristics (ROC) graph[34] to depict the prediction quality. This is a plot of the hit rate versus the false alarm rate, as a function of the total rate of alarms, which here is tuned by the threshold β_c . Only if in between the hit rate exceeds the false alarm rate, the predictor is useful. Random predictions generate equal hit and alarm rate, and hence they lead to the diagonal in ROC plot. Thus, only when the points lie above this diagonal the predictor is useful. As an example, the ROC graphs for $L = 512$ and $K = 1$ or $L = 256$ and $K = 2$ are shown in Fig. 3 (the rationale for choosing these two cases stems from the study of Ref.[35] in which it was shown that the OFC model with free boundary conditions exhibits in these cases -see their Fig.4- avalanche size distribution that agrees with the G-R law). For every given threshold value β_c and a target threshold Q_c , we get a point in this plot, thus varying β_c we get a curve. The various curves in Fig. 3 correspond to various values of $Q_c = 168, \dots, 1000$ increasing from the bottom to the top. An inspection of this figure shows that the points in each curve lie above the diagonal and the excess is higher for larger values of Q_c . In order to investigate the statistical validity of this result, we include in the same graph the results where: (a) the values of β_k were randomly shuffled

and the shuffled predictors were used (green curves) and (b) the time-series of Q_k was randomly shuffled and then β_k was estimated (magenta curves); in both cases, we obtain curves which almost coincide with the diagonal. This clearly demonstrates that the aforementioned excess of the results related with the original Q_k series from the diagonal comes from the sequential order of avalanches and cannot be considered as chancy.

We now proceed to the investigation of the temporal correlations between the magnitudes $m_k = \log_{10}(Q_k)/1.5$ obtained from the sizes Q_k of the avalanches in the OFC model preceding a large avalanche. The results can be visualized in two examples in Fig.4, where we plot in blue the exponent a_{DFA} of the detrended fluctuation analysis (DFA)[36] (along with the variability β plotted in red) versus the number W of avalanches before a large avalanche (negative x semi-axis, $x = -W$). Note that DFA has already been employed in Ref.[37] for monitoring temporal correlations before bifurcations. In the upper example, Fig.4(a), the value of a_{DFA} well before the large avalanche, being somewhat larger than 0.5, exhibits small changes but strongly increases upon approaching the large avalanche, i.e., at $W = 100$ the value of a_{DFA} becomes ≈ 0.75 which shows intensified *temporal* correlations. In the lower example, Fig.4(b), well before the large avalanche we have $a_{DFA} \approx 0.6$ showing long range temporal correlations, which first turn to anti-correlations upon approaching the large avalanche, e.g., $a_{DFA} \approx 0.43$ at $W = 400$, and finally become random, i.e., $a_{DFA} \approx 0.5$ at $W = 100$, just before the “mainshock”. In both examples of Fig.4, the variability β rapidly increases upon approaching a large avalanche showing clear precursory changes in the temporal correlations between avalanches’ magnitudes. A detailed statistical study of the OFC model ($K = 1, L = 512$), for $W = 100, 200, \dots 1000$, showed that among the 579 large ($Q_k > 30,000$) avalanches, only in 30% of the cases a rapid increase of β upon approaching them is observed. This is more or less consistent with empirical observations since in Japan this precursory increase was observed in 8 out of 25 earthquakes (all above M7 during 1 January 1994 to 11 March 2011 with depths smaller than 700 km)[26]. Concerning the α values, when studying $W = 100, 200, \dots 1000$, among the 579 large avalanches studied, in 76% of the cases the α value was found to become smaller than 0.5 (as seen in Fig.4(b)).

* **Correspondence to:** P. Varotsos (pvaro@otenet.gr)

[1] C. K. Peng, S. V. Buldyrev, A. L. Goldberger, S. Havlin, R. N. Mantegna, M. Simon, and H. E. Stanley,

- Physica A **221**, 180 (1995).
- [2] T. Kalisky, Y. Ashkenazy, and S. Havlin, Phys. Rev. E **72**, 011913 (2005).
- [3] J. W. Lamperti, Trans. Am. Math. Soc. **104**, 62 (1962).
- [4] A. Weron, K. Burnecki, S. Mercik, and K. Weron, Phys. Rev. E **71**, 016113 (2005); N. Scafetta and B. J. West, Complexity **10**, 51 (2005).
- [5] J. W. Kantelhardt, S. A. Zschiegner, E. Koscielny-Bunde, S. Havlin, A. Bunde, and H. E. Stanley, Physica A **316**, 87 (2002).
- [6] P. A. Varotsos, N. V. Sarlis, and E. S. Skordas, *NATURAL TIME ANALYSIS: THE NEW VIEW OF TIME. Precursory Seismic Electric Signals, Earthquakes and other Complex Time-Series* (Springer-Verlag, Berlin Heidelberg, 2011).
- [7] B. Gutenberg and C. F. Richter, *Seismicity of the Earth and Associated Phenomena* (Princeton Univ. Press, Princeton, New York, 1954).
- [8] R. Shcherbakov, D. L. Turcotte, and J. B. Rundle, Geophys. Res. Lett. **31**, L11613 (2004).
- [9] Q. Li, J. Cen, L. Yu, and B. Hao, Acta Geophys. Sinica **21**, 101 (1978); M. Imoto, Tectonophysics **193**, 311 (1991); Y. Tsukakoshi and K. Shimazaki, Earth Planets Space **60**, 915 (2008); K. Katsumata, Earth Planets Space **63**, 709 (2011).
- [10] J. Henderson and I. Main, Geophys. Res. Lett. **19**, 365 (1992).
- [11] P. A. Varotsos, N. V. Sarlis, and E. S. Skordas, Practica of Athens Academy **76**, 294 (2001); Phys. Rev. E **66**, 011902 (2002).
- [12] P. A. Varotsos, N. V. Sarlis, H. K. Tanaka, and E. S. Skordas, Phys. Rev. E **72**, 041103 (2005).
- [13] P. A. Varotsos, N. V. Sarlis, and E. S. Skordas, Phys. Rev. E **67**, 021109 (2003); *ibid* **68**, 031106 (2003).
- [14] P. Varotsos, K. Alexopoulos, and M. Lazaridou, Tectonophysics **224**, 1 (1993).
- [15] P. A. Varotsos, N. V. Sarlis, E. S. Skordas, H. K. Tanaka, and M. S. Lazaridou, Phys. Rev. E **74**, 021123 (2006).
- [16] H. Kanamori, Nature **271**, 411 (1978).
- [17] A. Corral, Phys. Rev. Lett. **92**, 108501 (2004); J. Davidsen and M. Paczuski, Phys. Rev. Lett. **94**, 048501 (2005); A. Saichev and D. Sornette, Phys. Rev. Lett. **97**, 078501 (2006).
- [18] J. R. Holliday, J. B. Rundle, D. L. Turcotte, W. Klein, K. F. Tiampo, and A. Donnellan, Phys. Rev. Lett. **97**, 238501 (2006).
- [19] J. F. Eichner, J. W. Kantelhardt, A. Bunde, and S. Havlin, Phys. Rev. E **75**, 011128 (2007); S. Lennartz,

- V. N. Livina, A. Bunde, and S. Havlin, EPL **81**, 69001 (2008).
- [20] E. Lippiello, L. de Arcangelis, and C. Godano, Phys. Rev. Lett. **103**, 038501 (2009); L. Telesca and M. Lovallo, Geophys. Res. Lett. **36**, L01308 (2009); N. V. Sarlis, E. S. Skordas, and P. A. Varotsos, Phys. Rev. E **80**, 022102 (2009); L. Telesca, Tectonophysics **494**, 155 (2010); M. Bottiglieri, L. de Arcangelis, C. Godano, and E. Lippiello, Phys. Rev. Lett. **104**, 158501 (2010).
- [21] S. Lennartz, A. Bunde, and D. L. Turcotte, Geophys. J. Int. **184**, 1214 (2011); V. N. Livina, S. Havlin, and A. Bunde, Phys. Rev. Lett. **95**, 208501 (2005); N. V. Sarlis, Phys. Rev. E **84**, 022101 (2011).
- [22] D. L. Turcotte, *Fractals and Chaos in Geology and Geophysics* (Cambridge University Press, Cambridge, 1997), 2nd ed.
- [23] P. A. Varotsos et al., Phys. Rev. E **73**, 031114 (2006); N. V. Sarlis, E. S. Skordas, M. S. Lazaridou, and P. A. Varotsos, Proc. Japan Acad., Ser. B **84**, 331 (2008).
- [24] See Supplemental Material at [URL will be inserted by publisher] for the identification of the occurrence time of an impending mainshock.
- [25] N. V. Sarlis, E. S. Skordas, and P. A. Varotsos, EPL **91**, 59001 (2010).
- [26] P. A. Varotsos, N. V. Sarlis, E. S. Skordas, S. Uyeda, M. Kamogawa, T. Nagao, and H. Tanaka, Proc. Jpn. Acad., Ser. B to be published (2012).
- [27] P. A. Varotsos, N. V. Sarlis, and E. S. Skordas, EPL **96**, 59002 (2011).
- [28] Z. Olami, H. J. S. Feder, and K. Christensen, Phys. Rev. Lett. **68**, 1244 (1992).
- [29] J. H. Dieterich and K. B. Richards-Dinger, Pure Appl. Geophys. **167**, 1087 (2010).
- [30] A. Helmstetter, S. Hergarten, and D. Sornette, Phys. Rev. E **70**, 046120 (2004).
- [31] R. Burridge and L. Knopoff, Bull. Seismol. Soc. Am. **57**, 341 (1967).
- [32] V. I. Keilis-Borok and I. M. Rotwain, Phys. Earth Planet. Inter. **61**, 57 (1990); V. I. Keilis-Borok and V. G. Kossobokov, Phys. Earth Planet. Inter. **61**, 73 (1990).
- [33] A. Garber, S. Hallerberg, and H. Kantz, Phys. Rev. E **80**, 026124 (2009).
- [34] T. Fawcett, Pattern Recogn. Lett. **27**, 861 (2006).
- [35] S. Lise and M. Paczuski, Phys. Rev. E **63**, 036111 (2001).
- [36] C.-K. Peng, S. V. Buldyrev, S. Havlin, M. Simons, H. E. Stanley, and A. L. Goldberger, Phys. Rev. E **49**, 1685 (1994).
- [37] V. N. Livina and T. M. Lenton, Geophys. Res. Lett. **34**, L03712 (2007).

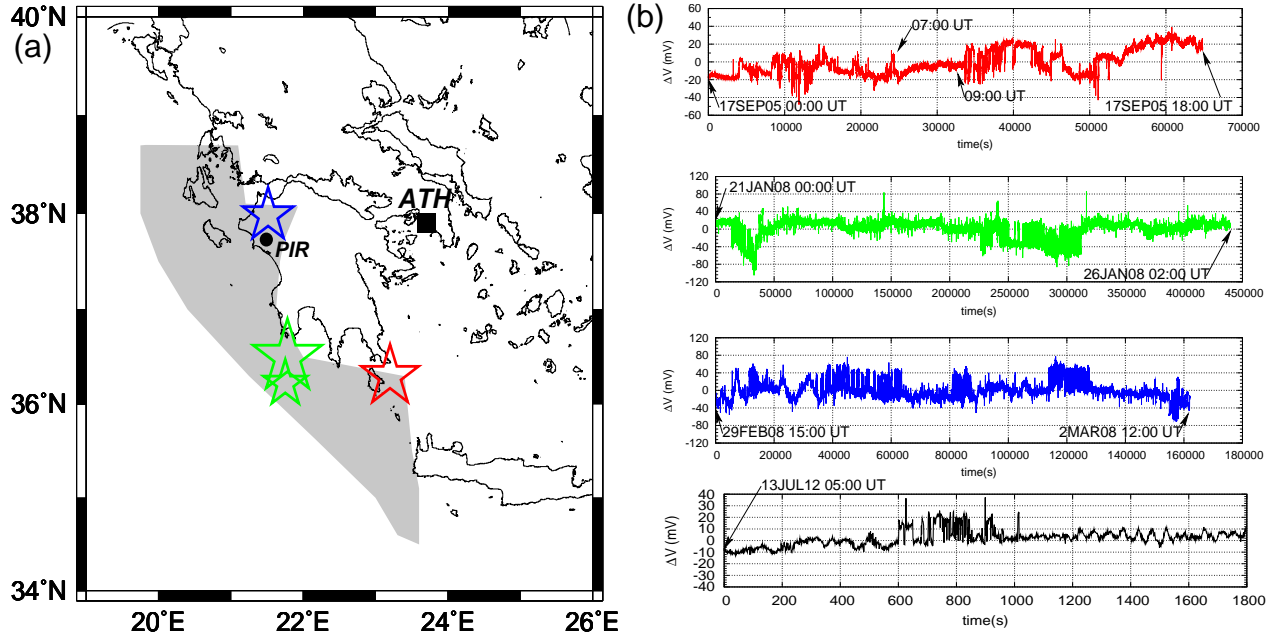


FIG. 1: (color online) (a) Major earthquakes in Greece on January 8, 2006 (red, magnitude $M_w = 6.7$), February 14, 2008 (green, $M_w = 6.9$ and 6.4) and June 8, 2008 (blue, $M_w = 6.4$) (b) Their preceding SES activities recorded at Pirgos (PIR) measuring station located in western Greece are shown (with the corresponding color) in the upper three channels. Earthquakes with SES activities at PIR are located in the shaded region of (a). Furthermore, an SES activity recorded at a station in northern Greece on July 13, 2012, is depicted in the lowest channel of (b).

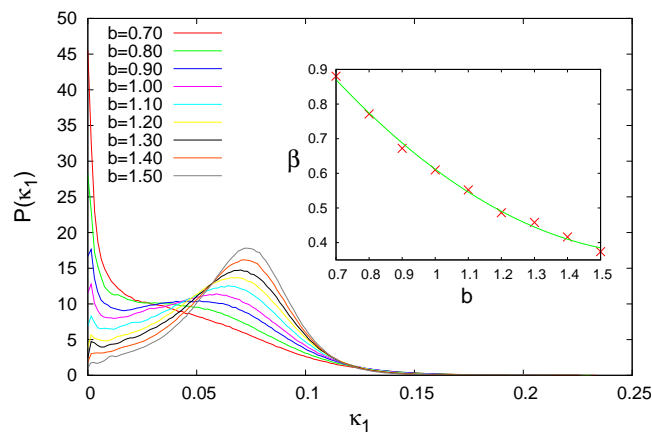


FIG. 2: (color online) The probability density function $P(\kappa_1)$ versus κ_1 for several values of b for temporally uncorrelated events obeying Eq.(4). The inset depicts the variability β as a function of b (the cross symbols refer to directly computed values, while the curve has been drawn as a guide to the eye).

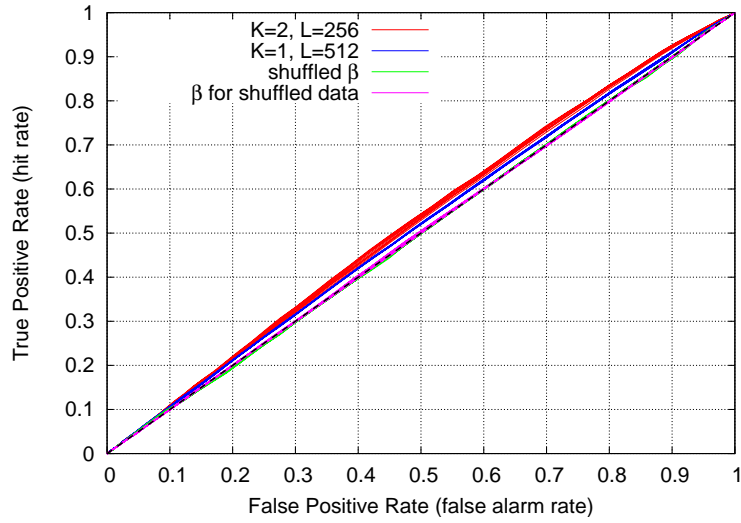


FIG. 3: (color online) The ROC diagram for the OFC earthquake model discussed in the text: red ($L = 256$ and $K = 2$) and blue ($L = 512$ and $K = 1$) lines. In addition, two ROC diagrams are depicted based on the results obtained for $L = 512$ and $K = 1$: The green curves correspond to the case when the values of β_k were randomly shuffled and the shuffled predictors were used, while the magenta curves when the time-series of Q_k was randomly shuffled and then β_k was estimated.

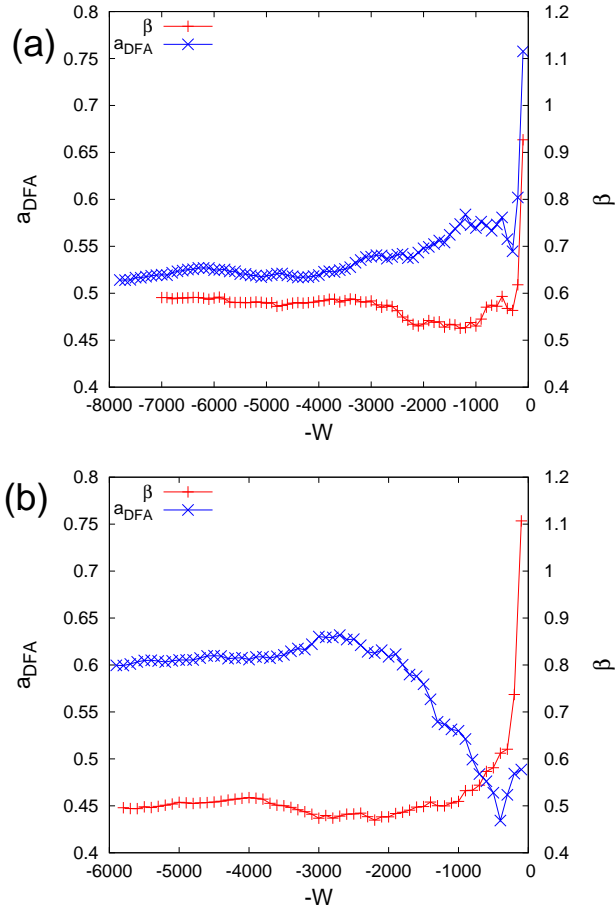


FIG. 4: (color online) The exponent a_{DFA} (blue, left scale) and the variability β (red, right scale) versus the number of the avalanches preceding a large avalanche, $Q_k = 40,325$ for (a) and $Q_k = 31,145$ for (b), that corresponds to $W = 0$ for the OFC model ($K = 1, L = 512$).